

Referee 1

1. *This manuscript describes a methodology for mapping magnetosheath locations relative to specific empirically-based models for the bow shock and magnetopause into an equivalent magnetosheath location with boundaries described by confocal paraboloids. Analytic solutions for plasma streamlines (and potential) and magnetic fields (and magnetic potential) can then be conformally mapped to a space bounded by more realistic boundaries.*

Reply (ref.01.01):

- No, not exactly. We are transforming the magnetosheath scalar potential not by a conformal mapping but by a non-conformal (and non-orthogonal) mapping in this manuscript. It is of course ideal if the harmonic functions (given as the solution of Laplace equation) were transformed into an arbitrarily-bounded magnetosheath using the conformal mapping. After extensive theoretical research (both analytically and numerically), it became clear that the conformal mapping of magnetosheath cannot be constructed uniquely. The reason for this is that the magnetosheath is not properly bounded for solving the Laplace equation. The magnetosheath is bounded only in the radial direction from the planet (or normal to the magnetopause) by the bow shock and the magnetopause. There is no boundary along the streamline, and the conformal mapping (Cauchy-Riemann condition or orthogonality condition) is no longer unique. Nevertheless, the algorithm we develop in the manuscript is a useful approach, because one can utilize the analytic solutions and the algorithm can relatively easily be implemented to various boundary shapes (though we chose only one example), which is of great help for future planetary research (missions and simulations). We highlight the problem with the conformal mapping in section 1 (page 2, lines 32–39) and section 5 (page 16, lines 314–320).

2. *In general, this article does not represent a significant advancement. It reads more like an Appendix of a larger study, with the Appendix detailing a technique to map locations between confocal, parabolic boundaries and empirically-based boundaries. While this technique is similar to previous efforts as described by Soucek and Escoubet [2012], Trattner et al., JGR [2015], and others, there is no effort here to demonstrate that this particular mapping technique better matches observations than previous techniques.*

Reply (ref.01.02):

- We accept the critique that the manuscript reads more like an appendix of a thesis. This impression comes from the slight mismatch between the manuscript goal (tool or algorithm development) and the journal scope (such as scientific message). We aim to develop a numerical grid scheme for space science applications. Numerical grid schemes are one of the favored discussion topics in fluid dynamics, computational physics, and informatics, but not so widely acknowledged in space science journals. See, for example, a grid generation using the conformal mapping by

Lin and Chandler-Wilde, J. Hydroinformatics, 2, 255–267, 2000 <https://doi.org/10.2166/hydro.2000.0023>. We nevertheless choose AnGeo for the dissemination of our study because the space science community should benefit the most from our algorithm development.

- The drawback with the radial mapping by Soucek and Escoubet (2012) is that the quality of mapping (distortion effect due to non-orthogonal grids) becomes quickly degraded in the flank to distant-tail region. Our mesh is robust against the distortion effect in the tail region. This point is elaborated in section 3 (pages 4–6) in the revised manuscript.

3. *Some of the references to empirical models of boundary shapes/sizes are inconsistent with the description provided here, or are examined under extremely specific solar wind conditions, or do not properly represent the knowledge of the physical boundaries far down the flank. Specifically,*

- (a) *The Farris et al., JGR [1991] empirical bow shock model is not a paraboloid model. It is an ellipsoid model (eccentricity of 0.81), describing the bow shock on the dayside. It is not a proper representation of the far flank bow shock.*
- (b) *The Cairns et al., JGR [1995] paraboloid bow shock model also does not properly represent the far flank bow shock. The distant bow shock shape approaches that of a hyperboloid.*
- (c) *The authors have selected a very specific exponent for the Shue et al., JGR [1997] model ($\alpha = 0.5$) in an effort to show that the analytic model is ‘simple’. The solar wind conditions for which this exponent is applicable (from the Shue et al. mode) is not often encountered (IMF $B_z \approx +8 \text{ nT}$, with specific values of solar wind dynamic pressure in order that $\alpha = 0.5$).*

Reply (ref.01.03):

- True and agreed. We added the referee’s comments (page 8, lines 160–164 and lines 170–172).

4. *Additional references to analytic models of the magnetosheath magnetic field (using expansions in Legendre polynomials) that make use of flexible magnetopause and bow shock boundary models (e.g., Romashets and Vandas, JGR, [2019]) should be provided and discussed.*

Reply (ref.01.04):

- Oh, thank you very much for introducing us this excellent paper! Yes, we cited the paper (page 16, lines 333–335).

5. *Although the claim is made in the manuscript that this technique can be applied to arbitrary boundary model shapes, it is not demonstrated that under general*

circumstances, the equations can be written in a closed form.

Reply (ref.01.05):

- Critique is well taken. We changed “arbitrary” into “non-parabolic” as we applied only one example (page 15, line 310).

6. *The technique described relies on determining the (straight line, or minimum) distance from a given point within the magnetosheath to the magnetopause. This is along the normal direction from the magnetopause. However, Lines 109–110 state that the task is to find the shell variable ‘v’ and the connector variable ‘u’ in the empirical magnetosheath. However, while the connector variable ‘u’ of the empirical magnetosheath is normal to the magnetopause surface, it is not a straight line through the magnetosheath? and doesn’t represent the minimum distance from the given point to the magnetopause. In other words, the distance from the magnetopause extends over a (narrow) range of connector variable ‘u’ values.*

Reply (ref.01.06):

- The confusion comes from the difference between the grids we used in the mapping (shown in figure 3, page 6, in the revised manuscript) and the u-v contours we showed in the original manuscript. We span the magnetopause-normal grids both in the KF model and in the empirical model, and here we see straight lines extending to the magnetopause.

7. *The rationale for the methodology described is confusing. For most implementations, the solar wind parameters are known, and the corresponding parameters at a given point within the magnetosheath are desired. However, the methodology here is to start with known parameters at a given place within the magnetosheath (relative to empirical models), conformal map to a location relative to the KF paraboloid boundaries, calculate the ‘u’ and ‘v’ values and determine the B-field, streamline, and potentials. The solar wind drivers appear to be missing. It appears that part of this strategy is based on the Toepfer et al. [2022] motivation; but a clear description for the order of steps for this technique is missing.*

Reply (ref.01.07):

- Yes, in the case of space plasma missions orbiting the Earth; But no, in the case of planetary mission (in which even the availability of plasma data is still challenging due to the mass, power budget, and telemetry budget). The advantage with the manuscript is that one can compute the magnetosheath potential for various scenarios of upstream conditions without extensive numerical efforts, assuming that the boundaries (bow shock and magnetopause) are well parametrized to the solar wind condition.

8. *Several of the equations presented are incorrect. For example, Eq.5 is infinite everywhere, due to the denominator. How are Eqs. 20 and 23 are used to derive Eq.24? Why do the units not match for the terms within Eq.39? How do Eqs.31-32 lead to Eq.33 when $ymp=0$?*

Reply (ref.01.08):

- Equation (5). Corrected (page 4, Eq. 13). Thank you!
- It is straightforward to derive Eq. (24) from Eq. (23), but Equation (24) offers an alternative approach to find the minimum distance to the brute-force method, but the manuscript can read even without this equation. Equation (24) was deleted in the revised manuscript.
- Equation (39). “2” should read “x” (page 11, Eq. 36). Thank you!
- Equations (31) becomes singular in the subsolar direction and Eq. (33) needs to be set separately to avoid the numerical divergence problem (page 10, lines 224–227).

Scalar-potential mapping of the steady-state magnetosheath model

Yasuhiro Narita¹, Simon Toepfer², and Daniel Schmid¹

¹Space Research Institute, Austrian Academy of Sciences, Schmiedlstr. 6, 8042 Graz, Austria

²Institut für Theoretische Physik, Technische Universität Braunschweig, Mendelssohnstr. 3, 38106 Braunschweig, Germany

Correspondence: Y. Narita (yasuhiro.narita@oeaw.ac.at)

Abstract. The steady-state magnetosheath model has various applications in studying the plasma and magnetic field profile around the planetary magnetospheres. In particular, the magnetosheath model is analytically obtained by solving the Laplace equation for parabolic boundaries (bow shock and magnetopause). We address the question “How can we utilize the magnetosheath model by transforming into a more general, empirical, non-parabolic magnetosheath geometry?”

5 To achieve the goal, we develop the scalar-potential mapping method which provides a semi-analytic estimate of steady-state flow velocity and magnetic field in the empirical magnetosheath domain. The method makes use of a coordinate transformation from the empirical magnetosheath domain into the parabolic magnetosheath domain, and evaluate a set of the shell variable and the connector variable to utilize the solutions of Laplace equation obtained for the parabolic magnetosheath domain. Our model uses two invariants of transformation: the zenith angle in the magnetosheath and the ratio of the distance to the magnetopause 10 to the thickness of magnetosheath along the magnetopause-normal direction. The use of magnetopause-normal direction makes a marked difference from the earlier model construction using the radial direction as reference. The plasma flow and magnetic field can be determined as a function of the upstream condition (flow velocity or magnetic field) in a wide range of zenith angle. The scalar-potential mapping method is computationally inexpensive by using the analytic expression as much as possible, is applicable to various planetary magnetosheath domains.

15 1 Introduction

Steady-state plasma flow and magnetic field can be regarded as a realization of potential field in the planetary magnetosheath region when the vorticity and the electric current are treated as ignored. In such a case, the potential is obtained by solving the Laplace equation, which was elegantly and analytically solved by Kobel and Flückiger (1994) for a parabolic shape of magnetosheath (hereafter KF). The KF potential was further extended to the stream function in the magnetosheath by Guicking 20 et al. (2012). The KF solution made a series of breakthroughs in the magnetosheath research. One of the most successful applications is the ability to track the plasma parcel along the streamline in the modeled magnetosheath. The tracking method was extensively used to observationally study the mirror mode growth (e.g., Tatrallyay et al., 2002; Génot et al., 2011) and the streamwise turbulence evolution in the magnetosheath (Guicking et al., 2012). Predictive models of plasma flow and magnetic field serve as a useful tool when combined with the numerical simulation or the observational data.

25 The KF potential is obtained on the assumption that the planetary bow shock and magnetopause have a parabolic shape sharing the same focal point. Empirical models of the bow shock and magnetopause (fitted to the spacecraft data), on the other

hand, are not necessarily parabolically or co-focally shaped. For example, the empirical Earth bow shock model by Farris et al. (1991) and Cairns et al. (1995) has a parabolic shape but the focal point differs from that of the KF solution; the empirical magnetopause model by Shue et al. (1997) applies a power-law scaling to the parabolic shape such that the magnetic field lines appear stretched in the tail region. The gap between the KF parabolic magnetosheath and the empirical magnetosheath needs to be filled when applying the KF potential in the empirical magnetosheath.

Naively speaking, one wishes to find a conformal mapping (angle-preserving mapping) from the KF parabolic magnetosheath onto a non-parabolic shape of empirical magnetosheath such as the analytic extension of magnetopause shape (Narita et al., 2023). However, no general mathematical algorithm is known so far to obtain the conformal mapping when the spatial domain is not properly bounded. The problem lies in the fact that the magnetosheath is bounded only by two sides, i.e., the standing shock and the magnetopause in the radial direction to the planet, but not bounded along the flow in the tail region. The algorithms of numerical conformal mapping are so far proposed for spatially bounded domains (Papamichael and Whiteman, 1973; Chakravarthy and Anderson, 1979; Fornberg, 1980; Karageorghis et al., 1996) or domains with a closed shape of internal boundaries (Wei et al., 2014).

Here we address the question “How can we utilize the KF magnetosheath model by transforming into a more general, empirical, non-parabolic magnetosheath geometry?” To achieve the goal, we develop a mapping method which provides a semi-analytic estimate of steady-state flow velocity and magnetic field in the empirical magnetosheath domain. Our scalar-potential mapping method is computationally inexpensive by using the analytic expression as much as possible, and is applicable to various planetary magnetosheath domains.

This work is organized in the following fashion. After reviewing the magnetosheath model constructed by Kobel and Flückiger (1994) (section 2 and discussing different mapping methods (section 3), the detailed procedure of the magnetopause-normal mapping is presented (section 4) with concluding remark (section 5).

2 Revisiting the magnetosheath scalar potential

2.1 Parabolic coordinates

In the KF parabolic coordinates, the shell variable v and the connector u play an important role in computing the flow velocity and magnetic field in the magnetosheath. These variables are explicitly evaluated using Cartesian coordinates and the radial distance from the focal point as

$$v = \sqrt{r_0 + (x_k - x_0)} \quad (1)$$

$$u = \sqrt{r_0 - (x_k - x_0)}, \quad (2)$$

where r_0 is the distance to the focus at x_0 :

$$r_0 = \sqrt{(x_k - x_0)^2 + y_k^2 + z_k^2}. \quad (3)$$

The focus is along the x axis, and is defined as

$$x_0 = \frac{1}{2} R_{\text{mp}}. \quad (4)$$

x_k , y_k , and z_k are the Cartesian representation of the KF magnetosheath model (i.e., with the pre-fixed bow shock and magne-

60 topause shapes) obtained by projecting the position vector onto the unit vectors e_x , e_y , and e_z :

$$x_k = \mathbf{r}^{(k)} \cdot \mathbf{e}_x \quad (5)$$

$$y_k = \mathbf{r}^{(k)} \cdot \mathbf{e}_y \quad (6)$$

$$z_k = \mathbf{r}^{(k)} \cdot \mathbf{e}_z. \quad (7)$$

To complete the variable set for computing the potentials and the stream function, the azimuthal angle ϕ is introduced as

$$65 \quad \phi = \text{atan}(z_k/y_k). \quad (8)$$

2.2 Velocity potential

In the frame of potential field theory, the flow velocity \mathbf{U} is obtained from the velocity potential (scalar potential) $\Phi^{(\text{vel})}$ as

$$\mathbf{U} = -\nabla\Phi^{(\text{vel})} = -\nabla \times (\Psi \mathbf{e}_\phi). \quad (9)$$

70 The symbol \mathbf{e}_ϕ is the unit vector in the azimuthal directions around the symmetry axis (Sun-to-planet direction). Kobel and Flückiger (1994) and Guicking et al. (2012) obtained the analytic expression of the velocity potential $\Phi^{(\text{vel})}$ using the shell variable v (iso-contour lines enveloping the magnetosphere) and the connector variable u (iso-contour lines connecting from the bow shock to the magnetopause).

$$75 \quad \Phi^{(\text{vel})} = -U_x \left(\frac{v_{\text{mp}}^2 v_{\text{bs}}^2}{v_{\text{bs}}^2 - v_{\text{mp}}^2} \right) \left(\frac{u^2 - v^2}{2v_{\text{bs}}^2} + \ln v \right) - \frac{1}{2} U_x (u^2 - v^2) + \Phi_0^{(\text{vel})}, \quad (10)$$

where U_x is the upstream flow velocity, v_{mp} the shell variable at the magnetopause, v_{bs} the shell variable at the bow shock, v the shell variable, u the connector variable, and $\Phi_0^{(\text{vel})}$ a free parameter (integration constant) which is set to zero without loss of generality. The boundary shell values v_{mp} and v_{bs} contain the information on the stand-off distances (R_{mp} and R_{bs}) in the subsolar region, and are defined by Kobel and Flückiger (1994) as

$$80 \quad v_{\text{mp}} = \sqrt{R_{\text{mp}}} \quad (11)$$

$$v_{\text{bs}} = \sqrt{2R_{\text{bs}} - R_{\text{mp}}}. \quad (12)$$

2.3 Stream function

Guicking et al. (2012) transformed the KF potential and obtained analytically the stream function Ψ as a function of the shell variable and the connector variable:

$$85 \quad \Psi = -\frac{1}{2} U_x \left(\frac{v_{\text{mp}}^2 v_{\text{bs}}^2}{v_{\text{bs}}^2 - v_{\text{mp}}^2} \right) \frac{u}{v} \left(\frac{v^2}{v_{\text{bs}}^2} - 1 \right) - \frac{1}{2} U_x u v. \quad (13)$$

Hereafter, one may set $U_x = -1$ so that the velocity potential $\Phi^{(\text{vel})}$ is normalized to the upstream velocity. Isocontour lines of the stream function represent the streamline.

2.4 Magnetic scalar potential

The magnetic field in the magnetosheath is derived from the scalar potential in the same fashion as the flow velocity, that is,

$$90 \quad \mathbf{B} = -\nabla\Phi^{(\text{mag})}. \quad (14)$$

The magnetic potential is a function of the shell variable v and the connector u (Kobel and Flückiger, 1994):

$$95 \quad \begin{aligned} \Phi^{(\text{mag})} = & -\frac{v_{\text{mp}}^2 v_{\text{bs}}^2}{v_{\text{bs}}^2 - v_{\text{mp}}^2} \times \\ & \left[\left(B_y^{(\text{up})} \cos \phi + B_z^{(\text{up})} \sin \phi \right) u \left(\frac{1}{v} + \frac{v}{v_{\text{bs}}^2} \right) + \right. \\ & \left. B_x^{(\text{up})} \left(\frac{u^2 - v^2}{2v_{\text{bs}}^2} + \ln v \right) \right] \\ & - B_x^{(\text{up})}(-x) - B_y^{(\text{up})}y - B_z^{(\text{up})}z + \Phi_0^{(\text{mag})}, \end{aligned} \quad (15)$$

where $B_x^{(\text{up})}$ is the sunward component of the upstream magnetic field (corresponding to the GSE-X in near-Earth space), and $B_y^{(\text{up})}$ and $B_z^{(\text{up})}$ are two components of the upstream magnetic field perpendicular to the x direction. ϕ is the azimuthal angle of the position around the symmetry axis (the y direction is given by the angle $\phi = 0$). The integration constant is chosen as $\Phi_0^{(\text{mag})} = 0$. The magnetic potential cannot be further transformed into the form of stream function since the magnetic field

100 distribution is essentially three-dimensional in the magnetosheath.

3 Mapping method comparison

3.1 Mapping problem

Our task is to find the shell variable v and the connector u in the empirical magnetosheath by finding a suitable mapping of the position vector from the empirical magnetosheath (denoted by \mathbf{r}) onto the KF parabolic system (denoted by $\mathbf{r}^{(k)}$). The evaluated v and u are then readily used to obtain the scalar potentials and the stream function. The flow velocity and the magnetic field in the empirical magnetosheath are obtained by computing the gradient of the respective potential.

110 A practically useful mapping procedure to utilize the KF potential is proposed by Soucek and Escoubet (2012) by using the radial direction as a reference. While the radial mapping can reasonably (i.e., with a relatively high accuracy) transform the KF potential into the empirical magnetosheath domain on the dayside, the mapping quality becomes degraded in the flank region due to the conversion effect associated with the non-orthogonal grid construction. Our approach makes a difference to the radial mapping in using the magnetopause-normal direction as a reference. The azimuthal coordinate ϕ is still orthogonal to the u and v coordinates. We briefly compare between the two mapping methods here.

3.2 Radial direction as reference

115 Soucek and Escoubet (2012) presented in their pioneering work an algorithm of radial mapping by transforming the KF magnetosheath model into a general, empirical magnetosheath shape by referring to the radial direction from the planet and scaling the radial position in the magnetosheath to the KF model. While the radial mapping can reasonably (i.e., with a relatively high accuracy) transform the KF potential into the empirical magnetosheath domain on the dayside, the mapping quality becomes degraded in the flank region due to the strongly non-orthogonal grids. Figure 1 displays a comparison of the 120 radial grids between the KF magnetosheath model and the empirical magnetosheath model. The grids span the radial direction to the planet and transfinite interpolation between the bow shock and the magnetopause. The radial mapping has a drawback in a stronger grid non-orthogonality effect, which causes an artificial converging flow pattern in the flank region (velocity potential shown in Fig. 2 when the scalar potential is directly transformed. In the Soucek-Escoubet method, the problem of flow conversion effect was avoided by solving the MHD Rankine-Hugoniot relation and tracking the streamline iteratively between the KF parabolic magnetosheath model and the empirical magnetosheath model.

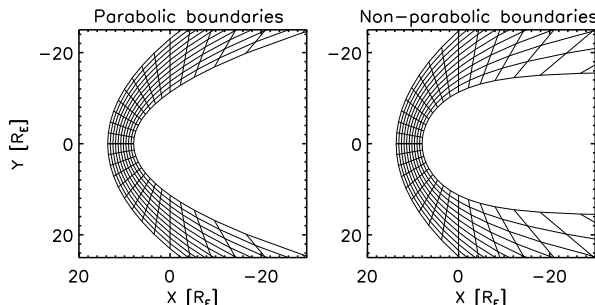


Figure 1. Grid pattern generated by the radial mapping for the Kobel-Flückiger parabolic magnetosheath (left panel) and the non-parabolic, empirical magnetosheath (right panel).

125 **3.3 Magnetopause-normal direction as reference**

Our mapping method makes a difference from the radial mapping method in that the magnetopause-normal direction is used as a reference to the magnetopause. Our method guarantees the grid orthogonality around the magnetopause both on the dayside and in the flank region. The magnetopause-normal grids are shown in Fig. 3 for the KF magnetosheath model (with parabolic

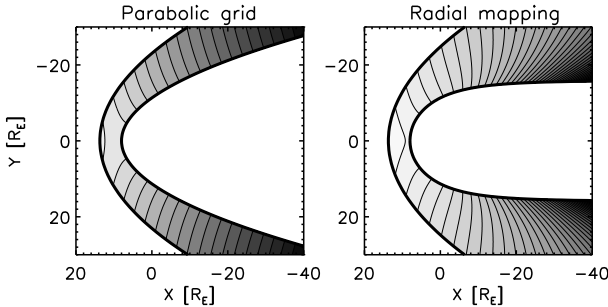


Figure 2. Velocity potential in the Kobel-Flückiger model (left panel) and its radial mapping onto the non-parabolic empirical boundaries (right panel).

boundaries) and the empirical magnetosheath model (with non-parabolic boundaries). Even though the exact conformal mapping is not available, the magnetopause-normal mapping method retains the grid orthogonality around the magnetopause. This feature (orthogonality around the magnetopause) plays a crucial role in mapping the scalar potentials. An example of the scalar-potential mapping by referring to the magnetopause-normal direction (our final results) are shown in section 4.8.

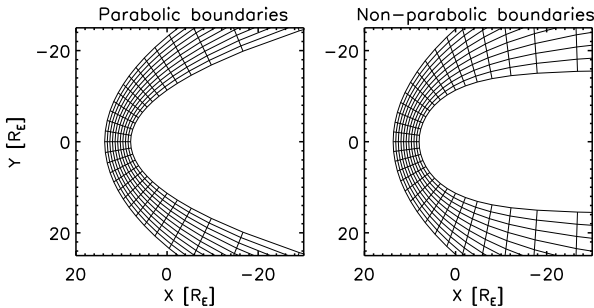


Figure 3. Mesh pattern used in the magnetopause-normal mapping in this work for the parabolic boundaries (left panel) and the non-parabolic, empirical boundaries (right panel).

4 Magnetopause-normal mapping

4.1 Overview of the procedure

The magnetopause-normal mapping is performed with two transformations. In the first transformation, the position vector is mapped from the empirical magnetosheath r onto the KF magnetosheath model r_k . This is achieved on the assumption that the distance to the magnetopause along the magnetopause-normal direction is the same when normalized to the magnetosheath thickness (defined as the distance from the magnetopause to the bow shock along the magnetopause-normal direction). The

azimuthal angle ϕ is the same between the empirical magnetosheath and the KF model. The first transformation is divided into 140 computing the distance to the magnetopause (step 1), the thickness of the empirical magnetosheath (step 2), the thickness of the KF magnetosheath (step 3), and the mapping of the position vector onto the KF model (step 4).

In the second transformation, the mapped position vector is used to compute the shell variable v and the connector variable 145 u (step 5) and to obtain the potentials and the stream function in the empirical magnetosheath using Eqs. (10), (13), and (15) (step 6). Here again, the azimuthal angle ϕ is treated as the same.

Figure 4 illustrates the mapping procedure and graphically explains the variables that need to be determined to perform the mapping such as the zenith angle of the nearest magnetopause θ_{mp} , the distance from the planet to the bow shock r_{bs} , the distance from the planet to the magnetopause r_{mp} , the relative distance to the magnetopause α_{emp} , and the magnetosheath thickness $\alpha_{emp}^{(bs)}$. The position vector r , the bow shock stand-off distance R_{bs} , the bow shock shape, the magnetopause stand-off distance R_{mp} , and the magnetopause shape are assumed to be known in our mapping.

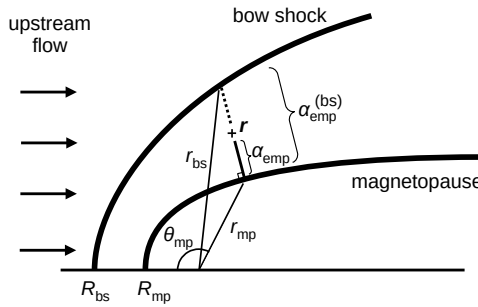


Figure 4. Variables used in the magnetopause-normal mapping with the zenith angle of the nearest magnetopause θ_{mp} , the radial distance to the bow shock and magnetopause along the magnetosheath-normal direction (r_{bs} and r_{mp} , respectively), the distance from the magnetosheath to the magnetopause α_{emp} , the magnetopause thickness $\alpha_{emp}^{(bs)}$. The position vector is denoted by r . The bow shock and magnetopause stand-off distances are denoted by R_{bs} and R_{mp} , respectively.

150 4.2 Setup

We begin with a position vector in the empirical magnetosheath domain, and express the position vector as $r = x\mathbf{e}_x + y\mathbf{e}_y + z\mathbf{e}_z$. Hereafter, we present the mapping procedure in the two-dimensional plane spanning the x and y directions for simplicity, but the computation in three dimensions is straightforward by representing the y component of position vector in the cylindrical fashion 155 as $\rho \cos \phi$ and the z component into $\rho \sin \phi$ using the distance ρ to the x axis. The boundaries (bow shock and magnetopause) are specified by the users and do not need to be parabolic. In this paper, we use the following bow shock and magnetopause models.

– The empirical bow shock position expressed in GSE (Geocentric Solar Ecliptic) coordinates proposed and discussed by Farris et al. (1991); Cairns et al. (1995)

$$x = R_{\text{bs}} - b_{\text{emp}} y^2, \quad (16)$$

160 where R_{bs} is the bow shock stand-off distance and b_{emp} is the empirical flaring parameter. We note here that the original Farris empirical bow shock model is not a paraboloid model, it is an ellipsoid model (with an eccentricity of 0.81), describing the bow shock on the dayside. It is not a proper representation of the far flank bow shock. Also, the Cairns paraboloid bow shock model does not properly represent the far flank bow shock. The distant bow shock shape approaches that of a hyperboloid.

165 – The empirical magnetopause position by Shue et al. (1997):

$$x^2 + y^2 - \frac{4R_{\text{mp}}^4}{4R_{\text{mp}}^2 - y^2} = 0, \quad (17)$$

in the Cartesian representation and

$$r_{\text{mp}} = R_{\text{mp}} \sqrt{\frac{2}{1 + \cos \theta}}. \quad (18)$$

in the polar representation.

170 We use a specific exponent for the Shue model (with an alpha exponent of 0.5) in an effort to show that the analytic model is ‘simple’. The solar wind conditions for which this exponent is applicable is not often encountered (e.g., interplanetary magnetic field has the B_z component larger than +8 nT, with specific values of solar wind dynamic pressure).

In our setup, the radial distance from the planet to the bow shock is expressed as (see appendix)

$$175 r_{\text{bs}} = \frac{1}{2b_{\text{emp}} \sin^2 \theta} \left(-\cos \theta + \sqrt{1 - (1 - 4b_{\text{emp}} R_{\text{bs}}) \sin^2 \theta} \right). \quad (19)$$

The radial distance to the magnetopause is given conveniently by Eq. (18). The Shue model reproduces the magnetopause stand-off distance R_{mp} in the subsolar direction ($\theta = 0$), and the cylindrical distance asymptotes to $2R_{\text{mp}}$ in the tail. It is worth noting here that one needs to compute the radial distance from the planet to the bow shock or magnetopause as a function of the zenith angle when using different shapes.

180 **4.3 Step 1: Measuring the distance to magnetopause**

In the first step, the distance from the given position in the magnetosheath to the nearest magnetopause is computed (see Fig. 5). We express the position vector along the magnetopause-normal direction such as

$$r = r_{\text{mp}} + \alpha_{\text{emp}} e_{\text{mp}}, \quad (20)$$

185 where \mathbf{r}_{mp} is the magnetopause position nearest to the position vector, and \mathbf{e}_{mp} is the unit vector in the magnetopause-normal direction. The unit vector points away from the planet and satisfies the condition

$$\mathbf{r}_{\text{mp}} \cdot \mathbf{e}_{\text{mp}} > 0 \quad (21)$$

The symbol α_{emp} is the distance to the magnetopause along the magnetopause-normal direction \mathbf{e}_{mp} in the empirical magnetosheath.

190 The nearest magnetopause position is obtained by searching for the zenith angle θ_{mp} for the minimum distance from the sample position to the magnetopause. The distance D is defined as

$$D = \sqrt{(r_x - r_{\text{mp}} \cos \theta_{\text{mp}})^2 + (r_y - r_{\text{mp}} \sin \theta_{\text{mp}})^2}. \quad (22)$$

The search for the minimum distance is implemented in a brute-force fashion as a function of $\mu_{\text{mp}} = \cos \theta_{\text{mp}}$ in our study.

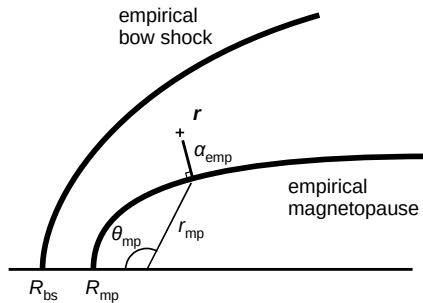


Figure 5. Measuring the distance to the empirical magnetopause (Step 1).

195 Having the nearest magnetopause at a distance of r_{mp} and a zenith angle of θ_{mp} , we are ready to compute the magnetopause-normal direction and the distance α_{emp} . To obtain the magnetopause-normal direction, we define the magnetopause shape function f_{mp} as

$$f_{\text{mp}} = x^2 + y^2 - \frac{4R_{\text{mp}}^4}{4R_{\text{mp}}^2 - y^2}, \quad (23)$$

and compute the normal direction by the gradient of f_{mp} as

$$\frac{\partial f_{\text{mp}}}{\partial x} = 2x \quad (24)$$

$$\frac{\partial f_{\text{mp}}}{\partial y} = 2y \left[1 - \frac{4R_{\text{mp}}^4}{(4R_{\text{mp}}^2 - y^2)^2} \right]. \quad (25)$$

200 The magnetopause-normal direction is obtained by normalizing the gradient vector $(\partial_x f_{\text{mp}}, \partial_y f_{\text{mp}})$ and representing with the basis vectors (\mathbf{e}_x and \mathbf{e}_y) as

$$\mathbf{e}_{\text{mp}} = \frac{\text{sgn}}{\sqrt{(\partial_x f_{\text{mp}})^2 + (\partial_y f_{\text{mp}})^2}} \times (\partial_x f_{\text{mp}} \mathbf{e}_x + \partial_y f_{\text{mp}} \mathbf{e}_y) \quad (26)$$

evaluated at the magnetopause ($x = r_{\text{mp}} \cos \theta_{\text{mp}}$ and $y = r_{\text{mp}} \sin \theta_{\text{mp}}$). The magnetopause-normal vector \mathbf{e}_{mp} has a unit length, 205 and the sign ($\text{sgn} = \pm 1$) is chosen such that the normal vector is pointing outward (Eq. 21). The distance α_{emp} to the magnetopause along the normal direction is obtained from Eq. (20) as

$$\alpha_{\text{emp}} = \frac{(x - r_{\text{mp}} \cos \theta_{\text{mp}}) + (y - r_{\text{mp}} \sin \theta_{\text{mp}})}{\mathbf{e}_{\text{mp}} \cdot \mathbf{e}_x + \mathbf{e}_{\text{mp}} \cdot \mathbf{e}_y} \quad (27)$$

Equation (27) is constructed to be robust against the singular behavior on the dayside ($\mathbf{e}_{\text{mp}} \cdot \mathbf{e}_y = 0$) and in distant tail ($\mathbf{e}_{\text{mp}} \cdot \mathbf{e}_x = 0$). 0.

210 4.4 Step 2: Computing the thickness of empirical magnetosheath

In the second step, the magnetosheath thickness is computed using the position vector and the magnetopause normal direction (Fig. 6). For our mapping purpose, the distance α_{emp} is normalized to the magnetosheath thickness $\alpha_{\text{emp}}^{(\text{bs})}$ such that the relative 215 distance $\alpha_{\text{emp}}/\alpha_{\text{emp}}^{(\text{bs})}$ serves as an invariant of the mapping from the empirical magnetosheath onto the KF magnetosheath. To achieve this, we combine Eq. (16) with Eq. (20), and analytically determine the thickness from the bow shock to the magnetopause in the empirical magnetosheath. That is, the thickness $\alpha_{\text{emp}}^{(\text{bs})}$ is obtained by rewriting the bow shock quadratic 220 equation (Eq. 16) for the position vector using the variable $\alpha_{\text{emp}}^{(\text{bs})}$ (Eq. 20) extended to the bow shock location. The equation is again quadratic, and the solution is algebraically obtained as:

$$\alpha_{\text{emp}}^{(\text{bs})} = \frac{1}{2b_{\text{emp}} e_{\text{mp},y}^2} \times [-(e_{\text{mp},x} + 2b_{\text{emp}} y_{\text{mp}} e_{\text{mp},y})^2 + d_{\alpha}], \quad (28)$$

220 where d_{α} is an auxiliary variable defined as

$$d_{\alpha} = [(e_{\text{mp},x} + 2b_{\text{emp}} y_{\text{mp}} e_{\text{mp},y})^2 - 4b_{\text{emp}} e_{\text{mp},y}^2 \times (x_{\text{mp}} + b_{\text{emp}} y_{\text{mp}}^2 - R_{\text{bs}})]^{1/2}. \quad (29)$$

In the subsolar direction ($y_{\text{mp}} = 0$), the thickness is simplified given as

$$225 \quad \alpha_{\text{emp}}^{(\text{bs})} = R_{\text{bs}} - R_{\text{mp}}. \quad (30)$$

Equations (28) becomes singular in the subsolar direction and Eq. (30) needs to be set separately to avoid the numerical divergence problem.

4.5 Step 3: Computing the magnetosheath thickness in the KF system

In the third step, the magnetosheath thickness is computed in the KF model (Fig. 7). We repeat the procedures of steps 1 and 2 230 for the KF system and determine the KF magnetosheath thickness as reference. We treat the zenith angle θ_{mp} and the relative distance $\alpha_{\text{emp}}/\alpha_{\text{emp}}^{(\text{bs})}$ as invariants of the mapping between the empirical magnetosheath and the KF system. The KF bow shock

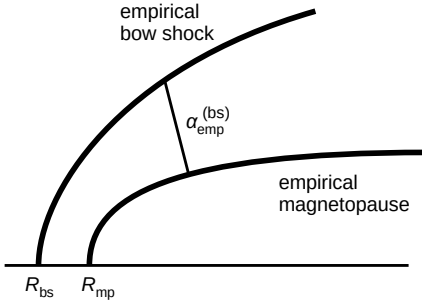


Figure 6. Computing the magnetosheath thickness in the empirical model (Step 2).

location is given as

$$x = R_{\text{bs}} - b_k y^2, \quad (31)$$

where the KF bow-shock flaring parameter b_k is pre-fixed as (Kobel and Flückiger, 1994)

$$235 \quad b_k = \frac{1}{4R_{\text{bs}} - 2R_{\text{mp}}}. \quad (32)$$

The radial distance from the planet to the KF bow shock is

$$r_{\text{bs}}^{(k)} = \frac{1}{2b_k \sin^2 \theta} \times \left(-\cos \theta + \sqrt{1 + (4b_k R_{\text{bs}} - 1) \sin^2 \theta} \right). \quad (33)$$

The KF magnetopause is defined in Kobel and Flückiger (1994) as

$$240 \quad x = R_{\text{mp}} - \frac{1}{2R_{\text{mp}}} y^2. \quad (34)$$

From Eq. (34) the radial distance from the planet to the KF magnetopause is computed as

$$r_{\text{mp}}^{(k)} = \frac{R_{\text{mp}}}{\sin^2 \theta} \left(-\cos \theta + \sqrt{1 + \sin^2 \theta} \right). \quad (35)$$

To obtain the magnetopause-normal direction in the KF system, we compute the gradient of the magnetopause shape function:

$$245 \quad f_{\text{mp}}^{(k)} = x - R_{\text{mp}} + \frac{1}{2R_{\text{mp}}} y^2. \quad (36)$$

The gradient is analytically given as

$$\frac{\partial f_{\text{mp}}^{(k)}}{\partial x} = 1 \quad (37)$$

$$\frac{\partial f_{\text{mp}}^{(k)}}{\partial y} = \frac{y}{R_{\text{mp}}} \quad (38)$$

The magnetopause-normal direction $e_{\text{mp}}^{(k)}$ is then obtained by applying Eqs. (37) and (38) to Eq. (26), which reads as

$$250 \quad e_{\text{mp}}^{(k)} = \frac{\text{sgn}}{\sqrt{(\partial_x f_{\text{mp}}^{(k)})^2 + (\partial_y f_{\text{mp}}^{(k)})^2}} \times \\ \left(\partial_x f_{\text{mp}}^{(k)} e_x + \partial_y f_{\text{mp}}^{(k)} e_y \right) \quad (39)$$

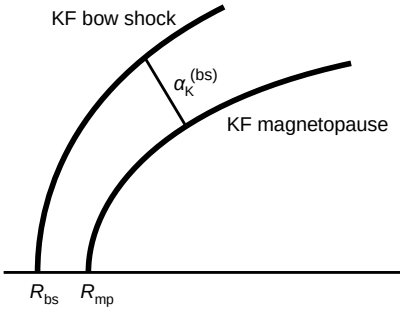


Figure 7. Computing the magnetosheath thickness in the KF model (Step 3). The same zenith angle as that in step 2 is used.

The thickness in the KF system $\alpha_k^{(\text{bs})}$ is determined by combining the bow shock shape (Eq. 31) with the position vector at the bow shock:

$$255 \quad \mathbf{r}_{\text{bs}}^{(k)} = \mathbf{r}_{\text{mp}}^{(k)} + \alpha_k^{(\text{bs})} e_{\text{mp}}^{(k)}. \quad (40)$$

Equation (31) becomes again a quadratic equation with respect to the thickness $\alpha_k^{(\text{bs})}$, and the solution reads:

$$\alpha_k^{(\text{bs})} = \frac{1}{2b_k e_{\text{mp},y}^2} \times \\ [-(e_{\text{mp},x} + 2b_k y_{\text{mp}} e_{\text{mp},y}) + d_{\alpha}^{(k)}] \quad (41)$$

where the auxiliary variable $d_{\alpha}^{(k)}$ is defined as

$$260 \quad d_{\alpha}^{(k)} = [(e_{\text{mp},x} + 2b_k y_{\text{mp}} e_{\text{mp},y})^2 - \\ - 4b_k e_{\text{mp},y}^2 (x_{\text{mp}} + b_k y_{\text{mp}}^2 - R_{\text{bs}})]^{1/2}. \quad (42)$$

4.6 Step 4: Mapping the position vector onto the KF system

In the fourth step, the mapping of the position vector is performed from the empirical magnetosheath onto the KF system (Fig. 8). Assumption is made such that the relative distance to the magnetopause along the magnetopause-normal direction 265 is the same between the two systems. The distance from the magnetosheath position vector to the magnetopause along the magnetopause-normal direction in the KF system α_k is then determined by the relative distance in the empirical magnetosheath α_{emp} , the thickness of the empirical magnetosheath $\alpha_{\text{emp}}^{\text{bs}}$, and magnetosheath thickness in the KF system $\alpha_k^{(\text{bs})}$ as

$$\alpha_k = \alpha_{\text{emp}} \alpha_k^{(\text{bs})} / \alpha_{\text{emp}}^{(\text{bs})}. \quad (43)$$

The mapped position vector is then computed as

270 $\mathbf{r}^{(k)} = \mathbf{r}_{\text{mp}}^{(k)} + \alpha_k \mathbf{e}_{\text{mp}}^{(k)}$, (44)

using the nearest magnetopause position $\mathbf{r}_{\text{mp}}^{(k)}$ (Eq. 35), the magnetosheath-to-magnetopause distance α_k (Eq. 43), and the magnetopause-normal direction $\mathbf{e}_{\text{mp}}^{(k)}$ (Eq. 39).

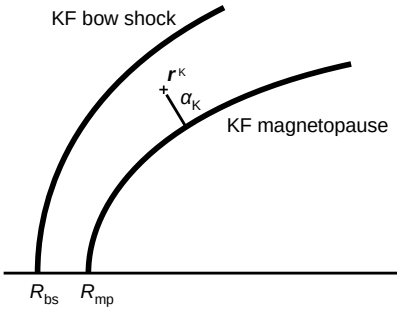


Figure 8. Mapping the position vector onto the KF magnetosheath model (Step 4).

4.7 Step 5: Evaluating the shell and connector variables

In the fifth step, the shell variable v and the connector variable u are computed from the mapped position vector $\mathbf{r}^{(k)}$ using Eqs. (1) and (2), respectively. The variables v and u are the same as the parabolic coordinates used in the KF potential with a focus at $x_0 = R_{\text{mp}}/2$. In our algorithm, the focus is explicitly given in Eqs. (1), (2), and (3). The azimuthal angle around the symmetry axis ϕ is treated in the same way as in the KF model.

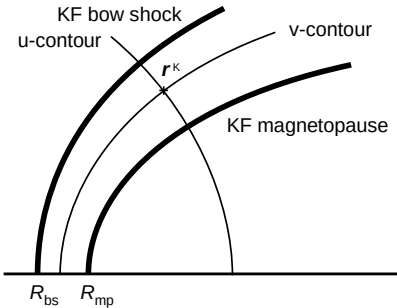


Figure 9. Evaluating the shell variable v and the connector variable u in the KF magnetosheath model (Step 5).

Figure 10 compares the iso-contours of the shell v and the connector u represented in the KF system (left panel) and the empirical magnetosheath (right panel) for a bow shock stand-off distance of $12.8 R_E$ (Génot et al., 2011), a bow shock flaring of $0.0223 R_E^{-1}$, (Farris et al., 1991; Cairns et al., 1995), and a magnetopause stand-off distance $9.8 R_E$ (Génot et al., 2011).

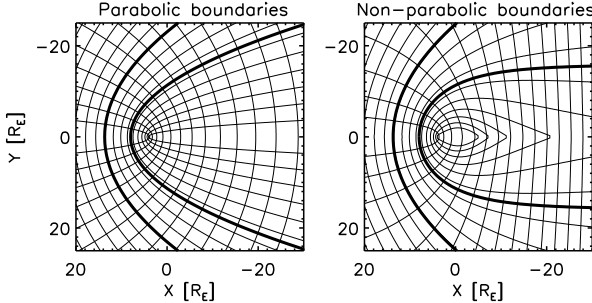


Figure 10. Iso-contour lines with $u = \text{const.}$ (center of curvature on the left side) and that with $v = \text{const.}$ (center of curvature on the right side) in the KF magnetosheath model (left panel) and the empirical magnetosheath model (right panel). The bow shock stand-off distance is 12.8 Earth radii and the magnetopause stand-off distance is 9.8 Earth radii.

The shell variable v is characterized by the lines with the curvature center on the right side in the panel, and contains the parabolic bow shock (at $v = v_{\text{bs}}$) and magnetopause (at $v = v_{\text{mp}}$) marked by thick lines. The connector variable u has the curvature center on the left side in the panel, and the iso-contour lines are orthogonal to the bow shock and magnetopause. [The computation of the \$u\$ and \$v\$ variables and their gradient and curl is performed in the Cartesian so that the connection represented by the Christoffel symbol vanish in the computation. Computation in the Cartesian domain is also beneficial to the practical application because spacecraft trajectories are often represented in the Cartesian coordinates.](#)

285

4.8 Step 6: Computing the potentials and stream function

The scalar potentials (velocity potential and magnetic potential) and the stream function are obtained from the shell v and the connector u using Eqs. (10), (13), and (15). The velocity potential (normalized to the upstream flow) is displayed in Fig. 11 left panel, and the stream function in right panel. The iso-contours of the velocity potential represent the lines of the same flow velocity. The iso-contours of the stream function represent the [streamlines](#) in the magnetosheath. The flow is deflected around the [nose of the magnetopause](#) (the subsolar point) and the streamlines are tangential to the magnetopause. [Due to the grid orthogonality around the magnetopause, the streamlines are constructed as tangential to the magnetopause shape, which qualifies the magnetopause-normal mapping method as a useful tool for the magnetosheath model.](#)

295

The magnetic potential and the derived magnetic field are displayed in Fig. 12. The magnetic potential and the magnetic field (the gradient of the potential multiplied by the minus sign) depend on the upstream field. Fig. 12 shows an example with an upstream field angle of 135 degree to the x axis (i.e., 45 degree to the upstream flow direction). The magnetic field is computed using the central difference scheme. Near the boundaries (bow shock or magnetopause), the mesh resolution is enhanced so that the mesh points do not cross the boundary when computing with the central difference scheme. The upstream field is deflected on the positive y side (right panel, lower half plane), and is draping the magnetopause on the negative y side (right panel, upper half plane).

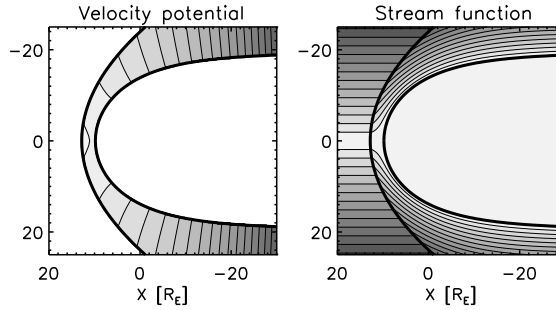


Figure 11. Velocity potential (left panel) and stream function (right panel) in the empirical magnetosheath domain obtained by mapping onto the shell variable v and the connector variable u .

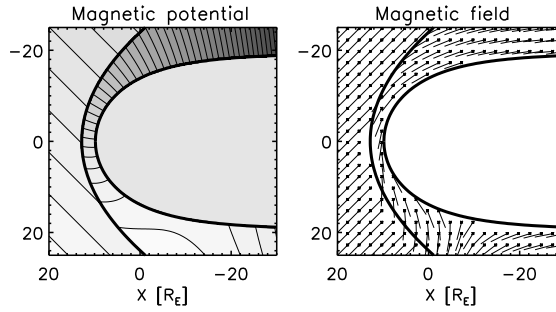


Figure 12. Magnetic potential for the upstream magnetic field with an angle of 135 degree to the x axis (45 degree to the upstream flow direction, (left panel) and sampled magnetic field vectors obtained by the negative gradient of the magnetic potential (right panel).

5 Concluding remark

Our potential mapping method may be regarded as an updated version of the radial mapping method (Soucek and Escoubet, 2012) by retaining the orthogonality near the magnetopause in the flank to tail region and also by computing the field through 305 the potential mapping. Velocity potential, stream function, and magnetic potential are evaluated in the empirical magnetosheath.

The advantages of our methods are as follows.

1. The method makes extensive use of the exact solution of the Laplace equation (the Kobel-Flückiger potential and the Guicking stream function). The plasma flow and magnetic field can be determined semi-analytically in a [wide range](#) of zenith angle in the magnetosheath when the [solar wind conditions](#) and the boundary shapes are given.
2. The method is applicable to a [non-parabolic shape](#) of magnetosheath domain, opening the door to develop a tool to assist numerical simulations and spacecraft observations of not only the Earth but also the planetary magnetosheath domain.
3. The method is computationally inexpensive. In particular, if the shape of bow shock and magnetopause is analytically given, most of the computational steps in the potential mapping method have an analytic expression.

As stated in section 1, one ideally needs to find a conformal mapping from the KF magnetosheath model onto the empirical magnetosheath. While the conformal mapping is known both for the empirical bow shock and the empirical magnetopause, the conformal mapping of the entire magnetosheath domain still remains a challenge. There are two problems on this. First, the closing boundary (the u -contours) connecting between the bow shock and the magnetopause is not known, and moreover, the uniqueness of finding such a boundary is not guaranteed. Second, the gradients along u are not the same between the empirical bow shock and the empirical magnetopause such that a naive transfinite interpolation ends up with highly non-orthogonal grids in the magnetosheath.

Our method of computing the plasma flow and magnetic field should be compared against the observations and simulations. For example, THEMIS and ARTEMIS spacecraft (Angelopoulos, 2008) and MMS spacecraft (Burch et al., 2016) are providing a huge amount of data on both sides of the bow shock in the equatorial plane; Cluster spacecraft Escoubet et al. (2001) are collecting data in polar orbit; ACE spacecraft data Stone et al. (1998) may be used as an upstream monitor; and Earth flyby data of planetary missions (such as Cassini, BepiColombo) cover the far-distance tail region. In reality, non-axisymmetric structure arises in the magnetosheath. Our method has the possibility to be extended to three-dimensional, non-axisymmetric modeling by the use of magnetopause normal mapping. It is possible to obtain the steady-state magnetosheath potential in a more general sense without referring to the KF94 solution. For example, for a non-axisymmetric geometry of magnetosheath (e.g., Dimmock and Nykyri, 2013), one may numerically solve the Laplace equation for a given set of boundary shapes (bow shock and magnetopause). Various numerical solvers are known for solving the Laplace equation such as the Jacobi method, the Gauss-Seidel method, and the successive over-relaxation (SOR) method. These Laplace solvers are numerically more expensive than the mapping method, but the computation in 3-D is feasible with the contemporary computational resources. Or one may expand the magnetosheath magnetic field in different orthogonal functions. The KF solution makes use of the Bessel functions (Kobel and Flückiger, 1994). For flexible magnetopause and bow shock boundary models, a magnetosheath magnetic field model is constructed by making use of Legendre polynomials (Romashets and Vandas, 2019). There is no restriction regarding the choice of the magnetopause model. The magnetopause-normal direction needs to be computed either analytically using the gradient of the magnetopause function as ∇f_{mp} , or numerically for a user-defined magnetopause shape.

Additional references to analytic models of the magnetosheath magnetic field (using expansions in Legendre polynomials) that make use of flexible magnetopause and bow shock boundary models (e.g., Romashets and Vandas, JGR, [2019])

340 Appendix: Planet-to-bow shock distance

By introducing the zenith angle θ and inserting $x = r_{bs} \cos \theta$ and $y = r_{bs} \sin \theta$ in Eq. 16), we obtain the equation for the radial distance to the empirical bow shock:

$$b_{\text{emp}} r_{\text{bs}}^2 \sin^2 \theta + r_{\text{bs}} \cos \theta - R_{\text{bs}} = 0. \quad (45)$$

Equation (45) can be algebraically solved, and we take the positive value of the solution as presented in Eq. (19).

345 *Code and data availability.* No codes or data are used in this work.

Author contributions. YN, ST, and DS developed the idea of potential mapping method, checked mathematics, and wrote the manuscript. YN prepared the figures. All authors listed have made a substantial, direct, and intellectual contribution to the work and approved it for publication.

Competing interests. Conflict of Interest: The authors declare that the research was conducted in the absence of any commercial or financial
350 relationships that could be construed as a potential conflict of interest.

References

Angelopoulos, V. The THEMIS mission, *Space Sci. Rev.*, 141, 5, 2008. <https://doi.org/10.1007/s11214-008-9336-1>

Burch, J. L., Moore, T. E., Torbert, R. B., and Giles, B. L., Magnetospheric Multiscale overview and science objectives, *Space Sci. Rev.*, 199, 5–21, 2016. <https://doi.org/10.1007/s11214-015-0164-9>

355 Cairns, I. H., Fairfield, D. H., Anderson, R. R., Carlton, V. E. H., Paularenas, K. I., and Lazarus, A.: Unusual locations of Earth's bow shock on September 24–25, 1987: Mach number effects, *J. Geophys. Res.*, 100, 47–62, 1995. <https://doi.org/10.1029/94JA01978>

Chakravarthy, S., and Anderson, D.: Numerical conformal mapping, *Math. Comp.* 33, 953–969, 1979.

Dimmock, A. P., and Nykyri, K: The statistical mapping of magnetosheath plasma properties based on THEMIS measurements in the magnetosheath interplanetary medium reference frame, *J. Geophys. Res. Space Physics*, 118, 4963–4976, 2013. <https://doi.org/10.1002/jgra.50465>

360 Escoubet, C. P., Fehringer, M., and Goldstein, M.: Introduction: The Cluster mission, *Ann. Geophys.*, 19, 1197–1200, 2001. <https://doi.org/10.5194/angeo-19-1197-2001>

Farris, M. H., Petrinec, S. M., and Russell, C. T.: The thickness of the magnetosheath – Constraints on the polytropic index, *Geophys. Res. Lett.*, 18, 1821–1824, 1991. <https://doi.org/10.1029/91GL02090>

365 Fornberg, B.: A numerical method for conformal mappings, *SIAM J. Sci. Stat. Comput.* 1, 386–400, 1980. <https://doi.org/10.1137/0901027>

Génot, V., Broussillou, L., Budnik, E., Hellinger, P., Trávníček, P. M., Lucek, E., and Dandouras, I.: Timing mirror structures observed by Cluster with a magnetosheath flow model, *Ann. Geophys.*, 29, 1849–1860, 2011. <https://doi.org/10.5194/angeo-29-1849-2011>

Guicking, L., Glassmeier, K.-H., Auster, H.-U., Narita, Y., and Kleindienst, G.: Low-frequency magnetic field fluctuations in Earth's plasma environment observed by THEMIS, *Ann. Geophys.*, 30, 1271–1283, 2012. <https://doi.org/10.5194/angeo-30-1271-2012>

370 Karageorghis, A., Stylianopoulos, N. S., and Zachariades, H. A.: A numerical conformal mapping method for harmonic mixed boundary value problems, *J. Sci. Comp.*, 11, 167–178, 1996. <https://doi.org/10.1007/BF02088814>

Kobel, E., and Flückiger, E. O.: A model of the steady state magnetic field in the magnetosheath, *J. Geophys. Res.*, 99, 23617–23622, 1994. <https://doi.org/10.1029/94JA01778>

Narita, Y., Toepfer, S., and Schmid, D.: Magnetopause as conformal mapping, *Ann. Geophys.*, 41, 87–91, 2023. <https://doi.org/10.5194/angeo-41-87-2023>

375 Papamichael, N., and Whiteman, J. R.: A numerical conformal transformation method for harmonic mixed boundary value problems in polygonal domains, *J. Applied Math.*, 24, 304–316, 1973. <https://doi.org/10.1007/BF01595198>

Romashets, E. P., and Vandas, M.: Analytic modeling of magnetic field in the magnetosheath and outer magnetosphere, *J. Geophys. Res. Space Physics*, 124, 2697–2710, 2019. <https://doi.org/10.1029/2018JA026006>

380 Schmid, D., Narita, Y., Plaschke, F., Volwerk, M., Nakamura, R., and Baumjohann, W.: Magnetosheath plasma flow model around Mercury, *Ann. Geophys.*, 39, 563–570, 2021. <https://doi.org/10.5194/angeo-39-563-2021>

Shue, J.-H., Chao, J. K., Fu, H. C., Russell, C. T., Song, P., Khurana, K. K., and Singer, H. J.: A new functional form to study the solar wind control of the magnetopause size and shape, *J. Geophys. Res. Space*, 102, 9497–9511, 1997. <https://doi.org/10.1029/97JA00196>

Soucek, J., and Escoubet, C. P.: Predictive model of magnetosheath plasma flow and its validation against Cluster and THEMIS data, *Ann. Geophys.*, 30, 973–982, 2012. <https://doi.org/angeo-30-973-2012>

385 Stone, E. C., Frandsen, A. M., Mewaldt, R. A., Christian, E. R., Margolies, D., Ormes, J. F., and Snow, F. The Advanced Composition Explorer, *Space Sci. Rev.*, 86, 1–22, 1998. <https://doi.org/10.1023/A:1005082526237>

Taírallyay, M. and Erdős, G.: The evolution of mirror mode fluctuations in the terrestrial magnetosheath, *Planet. Space Sci.*, 50, 593–599, 2002. [https://doi.org/10.1016/S0032-0633\(02\)00038-7](https://doi.org/10.1016/S0032-0633(02)00038-7)

390 Toepfer, S., Narita, Y., and Schmid, D.: Reconstruction of the interplanetary magnetic field from the magnetosheath data: A steady-state approach, *Front. Physics*, 10, 1050859 <https://doi.org/10.3389/fphy.2022.1050859>

Wei, L. K., Murid, A. H. M., and Hoe, Y. S.: Conformal mapping and periodic cubic spline interpolation, *Mathematika*, 30, 8–20, 2014.